

Detection of Low-Level Activities in Solar-Analog Stars from the Emission Strengths of Ca II 3934 Line *

Yoichi TAKEDA,¹ Akito TAJITSU,² Satoshi HONDA,³ Satoshi KAWANOMOTO,¹
Hiroyasu ANDO,¹ and Takashi SAKURAI¹

¹National Astronomical Observatory, 2-21-1 Osawa, Mitaka, Tokyo 181-8588
takeda.yoichi@nao.ac.jp, kawanomoto.satoshi@nao.ac.jp, ando.hys@nao.ac.jp,
sakurai@solar.mtk.nao.ac.jp

²Subaru Telescope, 650 North A'ohoku Place, Hilo, Hawaii 96720, U.S.A.
tajitsu@subaru.naoj.org

³Kwasan Observatory, Graduate School of Science, Kyoto University,
17 Ohmine-cho Kita Kazan, Yamashina-ku, Kyoto 607-8471
honda@kwasan.kyoto-u.ac.jp

(Received 2012 May 28; accepted 2012 June 25)

Abstract

Activity studies of solar-type stars, especially with reference to the status of our current Sun among them, have exposed the importance of (1) homogeneously selecting the sample stars and (2) reliably evaluating their activities down to a considerably low level. Motivated by these requirements, we conducted an extensive study on the activities of 118 solar-analog stars (of sufficiently similar properties to each other) by measuring the emission strength at the core of Ca II 3933.663 line (K line) on the high-dispersion spectrogram obtained by Subaru/HDS, where special attention was paid to correctly detecting the chromospheric emission by removing the wing-fitted photospheric profile calculated from the classical solar model atmosphere. This enabled us to detect low-level activities down to $\log R' \sim -5.4$ (R' is the ratio of the chromospheric core emission flux to the total bolometric flux), by which we could detect subtle activity differences which were indiscernible in previous studies. Regarding the Sun, we found $\log R'_{\odot} = -5.33$ near to the low end of the distribution, which means that it belongs to the distinctly low activity group among solar analogs. This excludes the once-suggested possibility for the high frequency of Maunder-minimum stars showing appreciably lower activities than the minimum-Sun.

Key words: stars: activity — stars: atmospheres — stars: solar-type — stars: rotation

1. Introduction

It is of great interest for solar as well as stellar astrophysicists to compare the activity of our Sun to those of a number of other similar solar-type stars, since it may provide us with an opportunity to infer the trend of solar activity on a very long astronomical time scale (i.e., investigating the long-time behavior of a star may be replaced by studying many similar stars at a given time).

Baliunas and Jastrow (1990) argued based on the results of Mt. Wilson Observatory's HK survey project for 74 solar-type stars that the distribution of S -index (nearly equivalent to $\propto \int_{\text{line}} F_{\lambda} d\lambda / \int_{\text{cont}} F_{\lambda} d\lambda$; i.e., the ratio of integrated core-flux of Ca II HK lines to the continuum flux; cf. Vaughan et al. 1978) is bimodal, with about 1/3 showing appreciably smaller activities than the Sun, which they interpreted as being in the “Maunder-minimum” state of activity. If this is true, it may mean that the spotless phase of considerably low-activity such as occurred in late 17th century in our Sun (Eddy 1976) may not necessarily be an unusual phenomenon in the long run.

However, this result could not be confirmed by a similar analysis done by Hall and Lockwood (2004), who reported based on many repeated observations of Ca II H and K lines for 57 Sun-like stars along with the Sun at Lowell Observatory that such a bimodal distribution of S -index (as suggesting the existence of a considerable fraction of appreciably lower activity stars than the current Sun) is not observed; actually, even the S -values of 10 “flat-activity” stars turned out to be comparable with (or somewhat larger than) the typical solar-minimum value.

Furthermore, Wright (2004) pointed out an important problem in Baliunas and Jastrow's (1990) sample selection. He concluded by examining the absolute magnitudes of their sample based on Hipparcos parallaxes that many of those “Maunder-minimum stars” with considerably low S indices are old stars evolved-off the main sequence, which suggests that their apparently low activity is nothing but due to the aging effect without any relevance to the cyclic or irregular change of activity in solar-type dwarfs. Thus, fairly speaking, the original claim by Baliunas and Jastrow (1990) appears to be rather premature and difficult to be justified from the viewpoint of these recent studies.

Yet, the issue of clarifying the status of solar activity

* Based on data collected at Subaru Telescope, which is operated by the National Astronomical Observatory of Japan.

among Sun-like stars does not seem to have been fully settled and further investigations still remain to be done:

— First, since understanding the activity of the Sun from a comprehensive perspective is in question, comparison samples should comprise stars as close to the Sun as possible. Admittedly, those authors surely paid attention to this point: Baliunas and Jastrow’s (1990) HK project targets were in the $B - V$ range of 0.60–0.76, while Hall and Lockwood’s (2004) Sun-like stars sample were chosen from stars of $0.58 \leq B - V \leq 0.72$, both narrowly encompassing the solar $(B - V)_{\odot}$ of 0.65 (Cox 2000). However, the homogeneity of these samples are not yet satisfactory. Could they be made up of further more Sun-like stars or solar analogs?

— Second, it appears that the precision of detecting low-level activity has been insufficient. Although Mt. Wilson S index reflects the core-emission strength (equivalent width) of Ca II HK lines, it would not be a sensitive activity indicator any more, when the emission becomes weak, as it stabilizes at a constant value determined by the photospheric absorption profile. While an indicator for the pure-emission strength, $R'_{\text{HK}} (\equiv R_{\text{HK}} - R_{\text{phot}}$; where $R_{\text{HK}} \equiv F_{\text{HK}}/F_{\text{bol}}$ and $R_{\text{phot}} \equiv F_{\text{phot}}/F_{\text{bol}}$), has also been introduced to rectify this shortcoming and widely used, the photospheric component R_{phot} is in most cases only roughly evaluated as a simple function of $B - V$ (e.g., Noyes et al. 1984) and thus its accuracy is rather questionable. Wright (2004) also pointed out the importance of correctly subtracting this component, in view of its possible dependence on other stellar parameters (i.e., not only on $B - V$ or T_{eff} , but also on $\log g$ and $[\text{Fe}/\text{H}]$).

These requirements motivated us to conduct a new investigation on this subject, since we have been engaged these years with the extensive study of 118 Sun-like stars selected by the criteria of $0.62 \lesssim B - V \lesssim 0.67$ and $4.5 \lesssim M_V \lesssim 5.1$ ($M_{V,\odot} = 4.82$; Cox 2000), a quantitatively as well as qualitatively ideal sample of solar-analog stars. This project was originally started for the purpose of clarifying the behavior of Li abundances ($A(\text{Li})$), and revealed that the rotational velocity ($v_e \sin i$) is the most influential key parameter (Takeda et al. 2007; hereinafter referred to as Paper I). In a successive study, we investigated the activities of these solar analogs by using the residual flux at the core of the Ca II 8542 line ($r_0(8542)$), and confirmed a clear correlation between $A(\text{Li})$, $v_e \sin i$, and $r_0(8542)$, as expected (Takeda et al. 2010; hereinafter referred to as Paper II). However, it turned out hard to discriminate the differences in $r_0(8542)$ when the activity is as low as that of the Sun, since it tends to get settled at ~ 0.2 and does not serve as a sensitive indicator any more. Actually, test calculations of non-LTE line formation suggested (cf. Appendix B in Paper II) that the core flux of the Ca II 8498/8542/8662 triplet lines are rather inert to the chromospheric temperature rise in the upper atmosphere when the activity is low, but that for the Ca II 3934/3968 doublet (H+K lines) is still sensitive and thus more advantageous for detecting the low-level activity. Then, we recently studied the Be abundances of these sample stars by using the Be II 3131 line based on the

near-UV spectra obtained with Subaru/HDS (Takeda et al. 2011; hereinafter referred to as Paper III). Since these HDS spectra fortunately cover the Ca II H+K lines in the violet region, we decided to reinvestigate the activities of these 118 Sun-like stars by measuring the core-emission strength of the Ca II 3934 (K) line, in order to clarify the activity status of our Sun in comparison with similar solar analogs, where special attention was given to correctly removing the background line profile computed from the solar photospheric model, while taking advantage of the fact that atmospheric parameters of all these targets are well established. The purpose of this paper is to report the outcome of this investigation.

2. Basic Observational Data

2.1. Target Sample

We use the same targets (118 solar analogs) as used in Papers I–III, which were selected by the criteria of having $B - V$ and M_V values sufficiently similar to those of the Sun ($|\Delta(B - V)| \lesssim 0.2\text{--}0.3$ and $|\Delta M_V| \lesssim 0.3$). See section 2 in Paper I for a detailed description about the sample selection. We also determined the atmospheric parameters (T_{eff} , $\log g$, v_t , and $[\text{Fe}/\text{H}]$) from the equivalent widths of Fe lines, and the stellar parameters (M and age) by comparing the positions on the HR diagram with the theoretical evolutionary tracks (cf. section 3 in Paper I). These parameters for most of the targets were actually confirmed to proximally distribute around the solar values (i.e., $|\Delta T_{\text{eff}}| \lesssim 100$ K, $|\Delta \log g| \lesssim 0.1$ dex, $|\Delta v_t| \lesssim 0.2$ km s $^{-1}$, $|\Delta [\text{Fe}/\text{H}]| \lesssim 0.2$ dex, $|\Delta M| \lesssim 0.1 M_{\odot}$, and $|\Delta \log age| \lesssim 0.5$ dex; cf. figures 4 and 5 in Paper I).

However, the following characteristics regarding the relations between these parameters are to be noted, which we had better bear in mind in discussing the behavior of stellar activities.

— Since the effect of a decreased metallicity on $B - V$ is compensated by a lowering of T_{eff} , several outlier stars with appreciably lower T_{eff} as well as $[\text{Fe}/\text{H}]$ ($\Delta T_{\text{eff}} \lesssim -200$ K and $[\text{Fe}/\text{H}] \lesssim -0.4$ dex) are included in our sample (cf. figure 4c in Paper I), such as HIP 26381, HIP 39506, HIP 40118, and HIP 113989; and they belong to the oldest group ($age \sim 10^{10}$ yr).

— These parameters are not independent from each other and some correlations appear to exist between specific combinations; such as age vs. T_{eff} (lower T_{eff} stars tend to be older), age vs. $[\text{Fe}/\text{H}]$ (lower $[\text{Fe}/\text{H}]$ stars tend to be older), M vs. age (lower-mass stars tend to be older), and v_t vs. T_{eff} (v_t tends to decrease with a lowered T_{eff}), as recognized from figure 5 or figure 10 in Paper I, though the existence of outlier stars mentioned above partly plays a role in these tendencies.

It should also be remarked that the data for HIP 41484 given in Paper I were incorrect, as reported in appendix A of Paper II, where the correct results derived from a reanalysis of this star are presented.

2.2. Observational Material

The spectroscopic observations of these 118 solar analogs and Vesta (substitute for the Sun) were carried out on 2009 August 6, 2009 November 27, 2010 February 4, and 2010 May 24 (Hawaii Standard Time), with the High Dispersion Spectrograph (HDS; Noguchi et al. 2002) placed at the Nasmyth platform of the 8.2-m Subaru Telescope atop Mauna Kea, by which we obtained high-dispersion spectra covering $\sim 3000\text{--}4600\text{ \AA}$ with a resolving power of $R \simeq 60000$. See section 2 of Paper III and electronic table E1 therein for details of the observations and the data reduction, as well as the basic data of the spectra (e.g., observing date, exposure time, S/N ratio at $\lambda \sim 3131\text{ \AA}$).

The counts of raw echelle spectra (including the effect of blaze function) around $\lambda \sim 3950\text{ \AA}$ (the broad maximum between the two large depressions of Ca II 3934 (K) and 3968 (H) lines) are typically about ~ 15 times as large as those at the UV region of $\lambda \sim 3131\text{ \AA}$, while the counts at core of the Ca II K line at 3934 \AA is about $\sim 10\%$ of those at $\lambda \sim 3950\text{ \AA}$. Therefore, the S/N ratio at the deep absorption core of the K line is not much different from the value at $\lambda \sim 3131\text{ \AA}$ given in electronic table E1 of Paper III; that is, on the order of $S/N \sim 100$.

3. Core Emission Measurement

3.1. K line of ionized calcium

Most activity studies of solar-type stars so far based on the core emission strengths of Ca II resonance lines appear to utilize both K (3934 \AA) and H (3968 \AA) lines, presumably due to the intention of reducing the systematic errors by averaging both two, since measurements tend to be done rather roughly by directly integrating raw spectra at the specified wavelength regions.

In this investigation, however, we focus only on the former K line at 3933.66 \AA , since (1) it is by two times stronger than the H line and thus comparatively more suitable as a probe of the condition at the optically-thin chromospheric layer, and (2) the latter Ca II H line at 3968.47 \AA is blended with the Balmer line (H ϵ at 3970.07 \AA) which would make the situation more complicated in simulating the photospheric profile to be subtracted.

Our spectra in the selected wavelength region ($3930\text{--}3937\text{ \AA}$) including the relevant Ca II K line are shown in figures 1 (Vesta/Sun), 2 (all 118 stars including Vesta/Sun), and 3 (all stars overplotted), where the continuum levels of the observed spectra are so adjusted as to match the theoretical ones as explained below. We can see from these figures that the strengths of core emission considerably vary from star to star, while that for the Sun is apparently weak.

3.2. Photospheric profile matching

Given that the very strong Ca II K and H lines with considerably extended damping wings are predominant at $\sim 3900\text{--}4000\text{ \AA}$, it is hopeless to empirically estab-

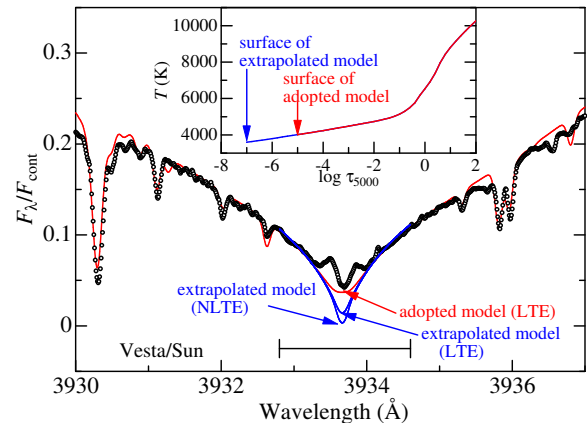


Fig. 1. Chromospheric emission feature at the core of the Ca II 3933.663 line for the case of the Sun (Vesta), in comparison with the theoretical photospheric spectra computed from the classical model atmosphere. Three solid lines indicate the theoretical residual flux spectra (normalized by the continuum flux), $r_{\lambda}^{\text{th}} (\equiv F_{\lambda}^{\text{th}} / F_{\text{cont}}^{\text{th}})$, which are based on essentially the same Kurucz's (1993) ATLAS9 solar atmospheric model but with different surface locations (i.e., the optical depth at the first mesh point), as depicted in the $T(\tau_{5000})$ structures shown in the inset. Red line is the LTE line profile derived from the adopted model atmosphere with its surface at $\log \tau_{5000} = -5$, while blue lines are the LTE and NLTE line profiles derived from the specially-extrapolated model atmosphere with its surface at $\log \tau_{5000} = -7$. Open symbols \dots r_{λ}^{obs} ($\equiv D_{\lambda}^{\text{obs}} / D_{\text{cont}}^{\text{obs}}$), where D_{λ}^{obs} is the actually recorded spectrum (ADU counts) while $D_{\text{cont}}^{\text{obs}}$ (regarded as an adjustable free parameter) was adequately chosen by requiring a satisfactory match between r_{λ}^{th} and r_{λ}^{obs} within $\lesssim 2\text{--}3\text{ \AA}$ from the line center (excepting the core-emission region) as explained in subsection 3.2. The specified line-core region ($3932.8\text{--}3934.6\text{ \AA}$) is indicated by a horizontal bar, over which the integration was made for evaluating the total chromospheric emission.

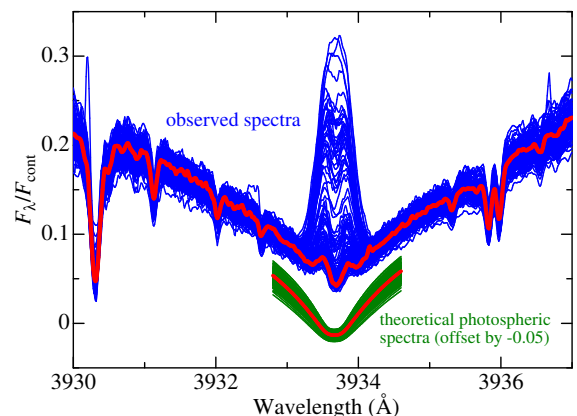


Fig. 3. In blue lines are overplotted the observed spectra (r_{λ}^{obs}) of Ca II 3933.663 in the $3930\text{--}3937\text{ \AA}$ region for all 118 stars (the same as those shown in figure 2), along with the Vesta/Sun spectrum highlighted in the red thick line. The theoretical photospheric spectra (r_{λ}^{th}) for each of the stars are also overplotted in green lines (only the solar spectrum is in red) with a downward offset by -0.05 . The wavelength scale of all spectra is adjusted to the laboratory frame.

lish the continuum position from the observed spectrum D_λ^{obs} (where an echelle order covers only ~ 50 Å). We thus “adjusted” the continuum position ($D_{\text{cont}}^{\text{obs}}$) of the spectrum (judged by eye-inspection) in such a way that $r_\lambda^{\text{obs}} (\equiv D_\lambda^{\text{obs}}/D_{\text{cont}}^{\text{obs}})$ satisfactorily matches the theoretically calculated residual flux $r_\lambda^{\text{th}} (\equiv F_\lambda^{\text{th}}/F_{\text{cont}}^{\text{th}})$ ¹ in the inner wing of the line (within $|\Delta\lambda| \lesssim 2\text{--}3$ Å from the line center, excepting the core-emission region). An example of such an accomplished match is displayed in figure 1 for the case of the Sun (Vesta).

Regarding the computation of theoretical spectra, we used Kurucz’s (1993) WIDTH9 program, which was modified by Y. Takeda to enable spectrum synthesis by including many lines. As to the atomic line data, we invoked Kurucz and Bell’s (1995) compilation and included all available lines in the relevant region. In particular, the data for the Ca II K line at 3933.663 Å of our primary concern are as follows: $\chi_{\text{low}} = 0.00$ eV, $\log gf = +0.134$, $\log \Gamma_{\text{R}} = 8.20$ [radiation damping width (s^{-1})], $\log \Gamma_e/N_e = -5.52$ [Stark effect damping width (s^{-1}) per electron density (cm^{-3}) at 10^4 K], and $\log \Gamma_w/N_{\text{H}} = -7.80$ [van der Waals damping width (s^{-1}) per hydrogen density (cm^{-3}) at 10^4 K]. Since the atmospheric parameters (T_{eff} , $\log g$, [Fe/H], and v_t) are already established (as summarized in table 1), the model atmosphere for each star was generated by 3-dimensionally interpolating Kurucz’s (1993) ATLAS9 model grids (LTE, plane-parallel model) in terms of T_{eff} , $\log g$, and [Fe/H]. Then, the synthetic spectrum was computed by using the relevant atmospheric model along with the metallicity-scaled abundances (for all elements including Ca; i.e., $[X/H] = [\text{Fe}/H]$ for any X) as well as the microturbulence (v_t), and further broadened according to the macrobroadening parameter determined in Paper III.

3.3. Evaluation of chromospheric emission

Now that the theoretical photospheric background profile (r_λ^{th}) used for subtraction has been successfully fitted with r_λ^{obs} by appropriately adjusting the continuum position, we can calculate the absolute emission flux (F'_{KP}) at the K-line core originating from the chromosphere (i.e., after subtraction of the photospheric component) as

$$F'_{\text{KP}} \equiv F_{\text{cont}}^{\text{th}} \int_{\lambda_1}^{\lambda_2} (r_\lambda^{\text{obs}} - r_\lambda^{\text{th}}) d\lambda \quad (1)$$

where λ_1 and λ_2 defining the integration range were chosen to be 3932.8 and 3934.6 Å, respectively (cf. figure 1). In order to demonstrate how this subtraction process works well, the photospheric profile (r_λ^{th}) at $[\lambda_1, \lambda_2]$ is displayed by red dashed line (along with the observed spectrum shown by symbols) for each star in figure 2. Finally, we can obtain R'_{KP} (the ratio of the chromospheric emission flux at the K line to the total bolometric flux) as

$$R'_{\text{KP}} \equiv F'_{\text{KP}}/F_{\text{bol}} = \pi F'_{\text{KP}}/(\sigma T_{\text{eff}}^4). \quad (2)$$

The resulting $\log R'_{\text{KP}}$ values for each of the 118 solar analogs (+Sun) are presented in table 1, where other activity-related quantities ($r_0(8542)$ and $v_e \sin i$) determined in Paper II are also given, along with the Li/Be abundances and stellar parameters established in Papers I and III.

3.4. Zero-Point Uncertainties in R'_{KP}

We would like to remark here that the “absolute” values of R'_{KP} are not very meaningful in the low-activity regime because of the uncertainties in its zero-point. That is, the theoretical profile we have computed for subtraction of the background photospheric component is by no means uniquely defined. Actually, apparently different results may be obtained depending on how it is calculated.

This situation is demonstrated in figure 1 for the solar case. The solar atmospheric model (which was obtained by interpolating the grids of Kurucz’s ATLAS9 model atmospheres) we adopted for calculating the LTE photospheric profile (red line) has its surface at $\log \tau_{5000}^{\text{surf}} = -5$ ($T^{\text{surf}} \sim 4000$ K). However, we note that the same but simply extrapolated model up to $\log \tau_{5000}^{\text{surf}} = -7$ ($T^{\text{surf}} \sim 3600$ K) yields an appreciably deeper core (upper blue line), reflecting the fact that the residual flux at the center is determined by $\sim B_\lambda(T^{\text{surf}})/B_\lambda(T^{\text{ph}})$ (T^{ph} : photospheric temperature) and very sensitive to T^{surf} in this violet region where Wien’s approximation nearly holds. Moreover, the core of the non-LTE profile (simulated by using the departure coefficients computed in Paper II for the case of Model E; cf. Appendix B therein) gets even more deeper approaching a completely dark core (lower blue line). Besides, the core shape strongly depends on the turbulent velocity field in the upper atmosphere; e.g., compare the non-LTE profile in figure 1 (computed with a depth-independent microturbulence of 1 km s^{-1}) with that for Model E depicted in figure B.1(b) of Paper II (where a variable microturbulent velocity field increasing with height was adopted).

Accordingly, R'_{KP} values [equation (2)] may be uncertain by an arbitrary constant, because $\int_{\lambda_1}^{\lambda_2} r_\lambda^{\text{th}} d\lambda$ in equation (1) can have different values depending on how r_λ^{th} is computed, though “relative” differences between R'_{KP} values of each star are surely meaningful as long as they are evaluated in the same system. Therefore, we should keep in mind that comparison of absolute values of our R'_{KP} with those of similar R' parameters derived by other groups, which we will try in subsection 4.1, is not much meaningful when the low-activity region (e.g., $\log R'_{\text{KP}} \lesssim -5$) is concerned. (On the other hand, such a zero-point problem should not be so serious for higher-activity cases, where $\log R'_{\text{KP}}$ tends to be dominated by the emission component and the role of r_λ^{th} subtraction is less significant.) In any event, we consider that our choice of shallower r_λ^{th} is adequate, since it leads to smaller values of R'_{KP} (as a result of larger subtraction), which eventually realizes a larger contrast in the $\log R'_{\text{KP}}$ values of

¹ We here use the astrophysical flux (F) defined by $\pi F_\lambda^{\text{th}} \equiv 2\pi \int_0^1 \mu I_\lambda^{\text{th}}(0, \mu) d\mu$, with which the effective temperature T_{eff} is related as $\pi F_{\text{bol}} = \pi \int_0^\infty F_\lambda d\lambda = \sigma T_{\text{eff}}^4$ (σ : Stephan–Boltzmann constant).

low-activity stars.

4. Discussion

4.1. Comparison of R'_{Kp} with previous studies

The $\log R'_{\text{Kp}}$ values determined in subsection 3.3 are compared with the equivalent activity indices² derived by Strassmeier et al. (2000) [$\log R'_K$], Wright et al. (2004) [$\log R'_{\text{HK}}$], and Isaacson and Fischer (2010) [$\log R'_{\text{HK}}$] in figures 4a, 4b, and 4c, respectively. These figures reveal almost the same tendency of correlation between our $\log R'$ and those of three studies: The agreement at $\log R' \gtrsim -5$ is mostly good, though our $\log R'$ tends to be slightly larger by ~ 0.1 dex for high-activity stars of $\log R' \gtrsim -4.5$. Meanwhile, a distinct difference is observed at the low-activity region where their $\log R'$ values tend to settle down at ~ -5 , while ours are dispersed over $-5.5 \lesssim \log R' \lesssim -5$. Admittedly, there is not much meaning in comparing the absolute R' values of different systems with each other, as remarked in subsection 3.4. The important point is, however, that we could detect the subtle difference in the low-level activity by measuring the weak core-emission at Ca II K with a careful subtraction of the background photospheric profile, while such a precision for distinguishing the delicate difference in the weak emission strength could not be accomplished by comparatively rough measurements in those previous studies.

4.2. Connection with stellar parameters

Figures 5a, 5b, and 5c display how the three activity-related parameters ($r_0(8542)$, $v_e \sin i$, and $\log \text{age}$; cf. Paper II) are correlated with $\log R'_{\text{Kp}}$.

We can observe in figure 5a a marked sensitivity-difference between $\log R'_{\text{Kp}}$ and $r_0(8542)$ in the low-activity region; i.e., the latter is inert to a variation of low-level activity and stabilizes at ~ 0.2 , despite that the former still shows an appreciable variability over $-5.5 \lesssim \log R'_{\text{Kp}} \lesssim -5$. This is just what we have expected (cf. Appendix B in Paper II), and demonstrates the superiority of the Ca II HK core emission (as long as correctly measured) to the line-center residual flux of Ca II 8542 when it comes to investigating the activities of solar-type stars as low as the Sun.

Figure 5b shows a positive correlation between R'_{Kp} and $v_e \sin i$, suggesting that stellar activity depends on the rotation rate, as we already confirmed in Paper II (cf. figure

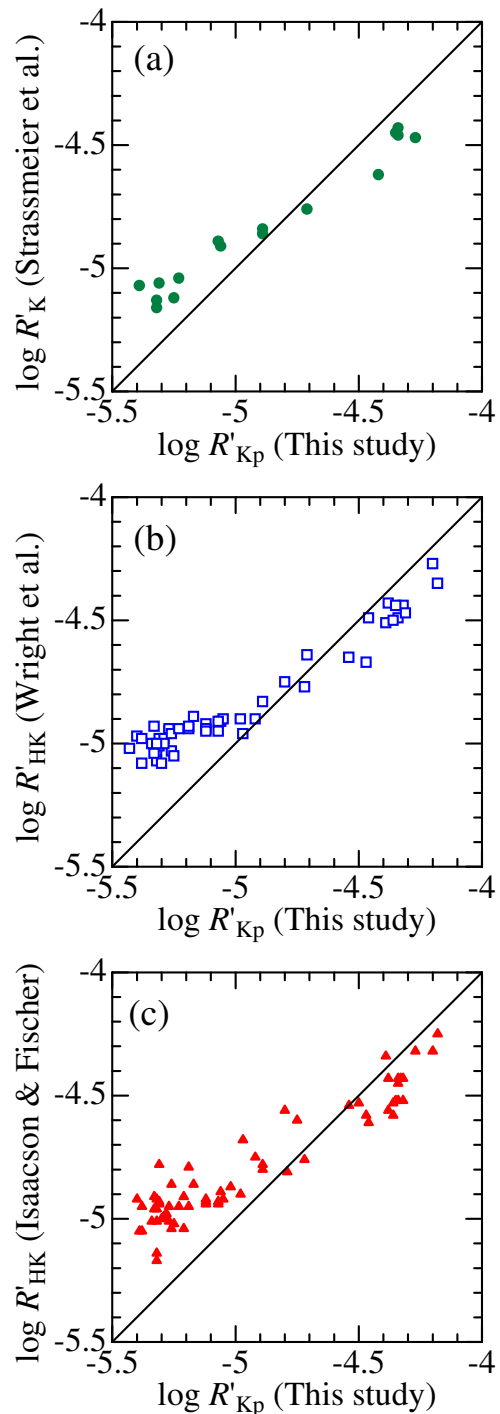


Fig. 4. Correlation of the $\log R'_{\text{Kp}}$ indices determined in this study with the literature values taken from three representative papers: (a) Strassmeier et al.'s (2000) $\log R'_K$ values, where 16 stars are in common. (b) Wright et al.'s (2004) $\log R'_{\text{HK}}$ values, where 50 stars are in common. (c) Isaacson and Fischer's (2010) $\log R'_{\text{HK}}$ values, where 66 stars are in common. (Since $\log R'_{\text{HK}}$ of Wright et al. (2004) as well as Isaacson and Fischer (2010) should be equivalent to the mean of $\log R'_H$ and $\log R'_K$, it may be directly compared with our $\log R'_{\text{Kp}}$.)

² Since Strassmeier et al. (2000) treated H and K lines separately and presented each data of F'_H and F'_K , we could convert their $R'_{\text{HK}}[\equiv (F'_H + F'_K)/F_{\text{bol}}]$ (as clearly defined by them) into $R'_K[\equiv F'_K/F_{\text{bol}}]$ which is directly comparable with our R'_{Kp} . Meanwhile, the R'_{HK} data derived by Wright et al.'s (2004) as well as Isaacson and Fischer (2010) appear to be essentially the *average* (not the sum) of R'_H and R'_K as judged by their extents. Therefore, we should be cautious about different definitions in the meaning of R'_{HK} . This situation is manifestly displayed in figure 7 of Paper II, where we can see that R'_{HK} (Strassmeier) is systematically larger than R'_{HK} (Wright) by 0.3 dex. Therefore, we compared our $\log R'_{\text{Kp}}$ with R'_{HK} (Wright, Isaacson) without applying any correction, since the latter is practically equivalent to R'_K in any case.

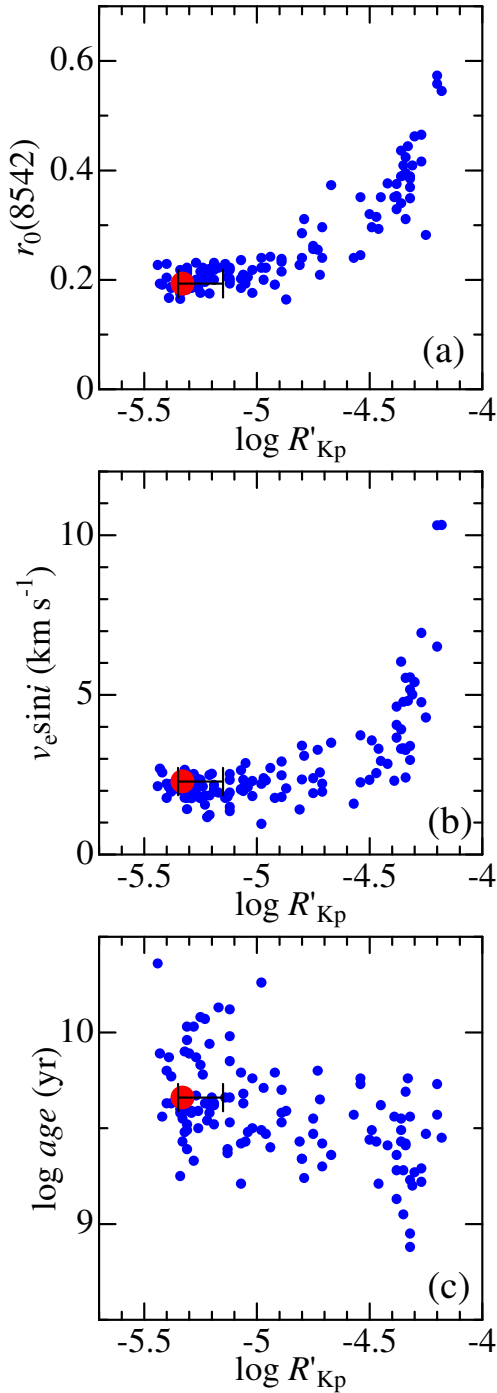


Fig. 5. Diagrams showing how the activity-related quantities derived in Paper I and Paper II ($r_0(8542)$, $v_e \sin i$, and $\log age$; also given in table 1) are correlated with the activity index ($\log R'_{Kp}$) derived in this study. (a) $r_0(8542)$ vs. $\log R'_{Kp}$, (b) $v_e \sin i$ vs. $\log R'_{Kp}$, and (c) $\log age$ vs. $\log R'_{Kp}$. The $\log R'_{Kp,\odot}$ value which we derived from the spectrum of Vesta/Sun (corresponding to the near-minimum phase of activity) is indicated by the bigger (red) circle, while the expected minimum–maximum range of $\log R'_{Kp,\odot}$ (between -5.35 and -5.15 ; cf. subsection 4.3) is shown by a horizontal bar.

5a therein). However, since $v_e \sin i$ values cluster around ~ 2 km s⁻¹ at $-5.5 \lesssim \log R'_{Kp} \lesssim -5$, we can not state much about whether this activity–rotation connection persists down to such a low-activity region (also, uncertainties in the projection factor prevent from a meaningful discussion).

When we compare the *age* vs. R'_{Kp} relation depicted in figure 5c with the similar $r_0(8542)$ vs. *age* plot (cf. figure 5c of Paper II), the anti-correlation is more clearly (or less unambiguously, to say the least) recognized in the present case, thanks to the extended dynamic range of the activity indicator for low-activity stars, though the dispersion is still considerably large.

How the abundances of Li and Be depend on R'_{Kp} determined in this study is illustrated in figure 6, where their dependences upon $r_0(8542)$ and $v_e \sin i$ already discussed in Papers II and III are also shown for comparison. We can see from figures 6a that the near-linear relation between $A(\text{Li})$ and $\log R'_{Kp}$ ($A(\text{Li}) \simeq 7 + \log R'_{Kp}$) holds widely from highly active ($\log R'_{Kp} \sim -4$) to less active ($\log R'_{Kp} \sim -5.5$) stars, in contrast to the case of $A(\text{Li})$ vs. $r_0(8542)$ where $A(\text{Li})$ shows a considerable dispersion at $r_0(8542) \sim 0.2$ (as if compressed) because of the less sensitivity of $r_0(8542)$. This substantiates the observational conclusion in Paper II (or corroborates its validity even for less-active cases) that $A(\text{Li})$ closely depends upon the stellar activity, which further lends support for our previous argument that the key parameter for controlling the surface lithium in solar-analog stars is the stellar rotation.

Regarding $A(\text{Be})$, we suspected in Paper III that the peculiar 4 stars showing drastically depleted Be (by $\gtrsim 2$ dex) in comparison with the solar abundance (while others have more or less near-solar Be) might be very slowly-rotating and thus less active star than the Sun. However, since these 4 stars have appreciably different $\log R'_{Kp}$ from each other ($-5.4 \lesssim \log R'_{Kp} \lesssim -4.9$; cf. figure 6a') and are not necessarily less active than the Sun, this speculation does not seem likely. Some other explanation would have to be sought for.

4.3. Activities of solar analogs and the Sun

We now discuss the activity trends of 118 solar analogs, with special attention paid to the status of our Sun among its close associates, as the main subject of this study. While our discussion is based on the $\log R'_{Kp}$ indices determined by ourselves, we should keep in mind that only one snapshot data is available for each star. This means that uncertainties due to possible time-variations of stellar activities (whichever cyclic or irregular) are inevitably involved. For example, the Mt. Wilson S value for the Sun varies over the range of $0.16 \lesssim S_{\odot} \lesssim 0.20$ (Baliunas et al. 1995), which may be translated into a variability in $\log R'_{\odot}$ by ~ 0.2 dex ($-5.0 \lesssim \log R'_{\odot} \lesssim -4.8$) according to the transformation formula given by Noyes et al. (1984). Since the observation time (2010 February 5) of our solar spectrum (Vesta) had better be regarded as corresponding to the near-minimum phase because of the appreciably retarded beginning of cycle 24 after the minimum in

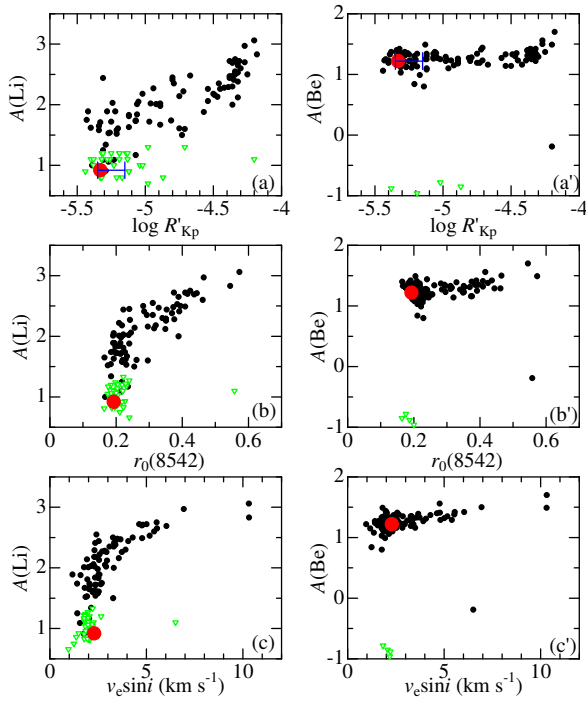


Fig. 6. Abundances of Li (left panels) and Be (right panels) plotted against $\log R'_{Kp}$ (top), $r_0(8542)$ (middle), and $v_e \sin i$ (bottom). The solar values are indicated by the bigger (red) circle in each panel. The expected minimum–maximum range of $\log R'_{Kp, \odot}$ is shown by a horizontal bar. The results for the determinable cases are shown by filled circles, while the open triangles denote the upper limits for the unmeasurable cases.

2008, our $\log R'_{Kp, \odot} (= -5.33)$ may as well be raised by $\lesssim 0.2$ dex at the solar maximum phase. It is thus reasonable to assume that our $\log R'_{Kp, \odot}$ ranges from -5.35 (solar minimum) to -5.15 (solar maximum), as indicated by a short horizontal bar in figures 5, 6, and 7.

The distribution histogram of $\log R'_{Kp}$ for all the 118 stars (and the Sun) and a similar histogram of $r_0(8542)$ (for comparison; cf. Paper II) are shown in figures 7a and 7b, respectively. We immediately notice in figure 7a the bimodal distribution of $\log R'_{Kp}$ having two peaks at ~ -5.3 and ~ -4.3 , constituting a well-known Vaughan–Preston gap (Vaughan & Preston 1980), while this bimodal trend is not clear in the distribution of $r_0(8542)$ (figure 7b) because of the densely peaked population around $r_0(8542) \sim 0.2$, reflecting its insensitivity when the activity is low (cf. figure 5a).

As we can see from figure 7a, the Sun with $\log R'_{Kp, \odot}$ of -5.33 manifestly belongs to the low-activity group (ranging from ~ -5.4 to ~ -5.0). As a matter of fact, only 11 ($\sim 10\%$)³ out of 118 solar analogs have $\log R'_{Kp}$ values

³ This ratio naturally depends on the reference solar activity, which may be subject to uncertainties due to cyclic variations as mentioned at the beginning of subsection 4.3. For example, if we assume a somewhat higher value of -5.2 for $\log R'_{Kp, \odot}$ corresponding to the active phase of the Sun, this fraction becomes

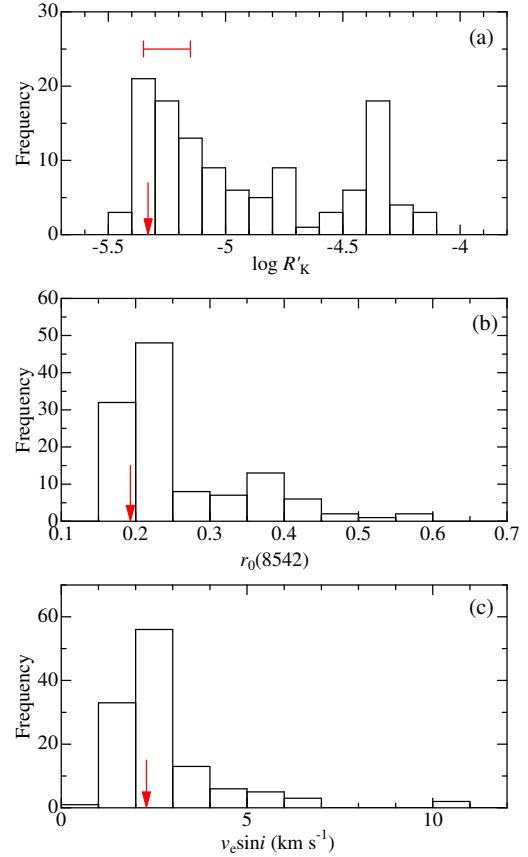


Fig. 7. Histograms showing the distributions of (a) $\log R'_{Kp}$ and (b) $r_0(8542)$ for our sample of 118 solar analogs. The position for the solar value is indicated by an downward arrow at each panel. The expected minimum–maximum range of $\log R'_{Kp, \odot}$ is shown by a horizontal bar.

smaller than -5.33 . This distinctly low-activity nature of the Sun is also recognized by eye-inspection of figure 2, revealing that the Ca II K line emission strength in our solar spectrum is near to the minimum level among other stars.

Thus, we can rule out the possibility for the existence of a significant fraction of Maunder-minimum stars (i.e., solar-type stars with appreciably lower activity than the Sun, even showing an another peak well below the current solar-minimum level), such as those once suggested by Baliunas and Jastrow (1990). This result corroborates the arguments raised by recent studies (e.g., Hall & Lockwood 2004; Wright 2004), which cast doubts about the reality of such a high frequency of Maunder-minimum stars. Thus, our Sun belongs to the group of manifestly low activity level among solar analogs, the fraction of stars below which is essentially insignificant.

4.4. Stars of Subsolar Activity

Although we have concluded that the Sun belongs to nearly the lowest activity group, some stars do exist show-

$\sim 30\%$.

ing activities still lower than that of the minimum-Sun, which are worth being examined more in detail. Since we defined that solar $\log R'_{\text{Kp},\odot}$ varies from -5.35 (minimum) to -5.15 (maximum) (cf. section 4.1), such stars may be sorted out by the criterion of $\log R'_{\text{Kp}} < -5.35$, which resulted in the following 8 objects ($\log R'_{\text{Kp}}$, $A(\text{Li})$, $\log \text{age}$, $[\text{Fe}/\text{H}]$, remark): HIP 7918 (-5.42 , 1.89, 9.56, $+0.01$), HIP 31965 (-5.39 , 1.00, 9.87, $+0.05$), HIP 39506 (-5.44 , < 0.9 , 10.36, -0.62) HIP 53721 (-5.43 , 1.75, 9.89, -0.02 , PHS), HIP 59610 (-5.40 , 1.62, 9.63, -0.06 , PHS), HIP 64150 (-5.38 , < 1.0 , 9.63, $+0.05$, Be depleted), HIP 64747 (-5.40 , < 1.1 , 9.80, -0.18), and HIP 96901 (-5.38 , < 1.1 , 9.77, $+0.08$, PHS).

While only one (HIP 39506) of these is an outlier of lower $[\text{Fe}/\text{H}]$ as well as lower T_{eff} (belonging to rather old population) as mentioned in subsection 2.1, the remaining 7 stars are Sun-like stars with sufficiently similar parameters, which excludes the possibility of such a low-level activity being due to stellar-evolution (i.e., evolved subgiants; cf. section 1).

We note here that (1) three (out of only five in our sample of 118 stars) planet-host stars are included, (2) all these stars have low-scale Li abundances ($A(\text{Li}) \lesssim 2$), and (3) their ages are similar to or older than that of the Sun. Combining these facts with the consequences in Papers I and II, we consider that these stars have actually low activities even compared with the solar-minimum level, and this is presumably attributed to their intrinsically slow rotation (which is closely related with the Li abundance as well as with the existence of giant planets).

It is, therefore, interesting to investigate the variabilities of these low-activity stars by long-term monitoring observations, in order to see how their activities behave with time (cyclic? flat? irregular?). Admittedly, activity observations for these stars have been reported in several published studies so far, for example: HIP 7918, 53721, 64150, and 96901 by Duncan et al. (1991); HIP 53721, 59610, 64150, and 96901 by Wright et al. (2004); HIP 7918, 53721, and 96901 by Hall et al. (2007); HIP 31965, 59610, 64150, and 96901 by Isaacson and Fischer (2010). However, as they are still quantitatively insufficient for establishing the long-term behavior of their activities⁴, much more observations are evidently needed.

5. Conclusion

There have been several arguments regarding the status of solar activity among similar Sun-like stars. which began with the implication of Baliunas and Jastrow (1990) based on their Mt. Wilson HK survey project that a considerable portion ($\sim 1/3$) of solar-type stars have activities significantly lower than the present-day Sun, which they called ‘‘Maunder-minimum stars.’’ However, their conclusion could not be confirmed by Hall and Lockwood’s

(2004) follow-up study, and Wright (2004) criticized the reality of such considerably low-active solar-type stars by pointing out that most of them are not so much dwarfs as evolved subgiants.

Given this controversial situation, we decided to contend with this problem by ourselves based on carefully selected sample of 118 solar-analogs sufficiently similar to each other (which we already investigated their stellar parameters as well as Li/Be abundances in a series of our previous papers), with a special attention being paid to reliably evaluating their activities down to a considerably low level.

Practically, we measured the emission strength at the core of Ca II 3933.663 line (K line) on the high-dispersion spectrogram obtained by Subaru/HDS, where we gave effort to correctly evaluating the pure emission component by removing the wing-fitted photospheric profile calculated from the classical solar model atmosphere, which enabled us to detect low-level activities down to $\log R'_{\text{Kp}} \sim -5.5$.

A comparison of our $\log R'_{\text{Kp}}$ results with the corresponding $\log R'$ values of Strassmeier et al. (2000), Wright et al. (2004), and Isaacson and Fischer (2010) revealed that low-active stars (for which they derived $\log R' \sim -5.1$ at the minimum limit) actually have a dispersion of ~ 0.4 dex ($-5.5 \lesssim \log R'_{\text{Kp}} \lesssim -5.0$) in our measurement, suggesting that our $\log R'_{\text{Kp}}$ has a higher sensitivity and thus advantageous. A similar situation holds regarding the comparison with $r_0(8542)$ we used in Paper II; i.e., this index stabilizes at ~ 0.2 and becomes insensitive for low-active stars in contrast to $\log R'_{\text{Kp}}$.

As another merit of using $\log R'_{\text{Kp}}$, we can state that the visibility of the $A(\text{Li})$ –activity relation as well as the age–activity relation becomes comparatively clearer, because this activity index turns out to have well diversified values for low-activity stars thanks to its high sensitivity, which can not be accomplished by using, e.g., $r_0(8542)$.

From the distribution histogram of $\log R'_{\text{Kp}}$, we could recognize a clear Vaughan–Preston gap between two peaks at ~ -5.3 and ~ -4.3 . Our result of $\log R'_{\text{Kp},\odot} = -5.33$ manifestly suggests that the Sun belongs to the group of the former peak and has a distinctly low-active nature among solar analogs. Actually, a fraction of stars with $\log R'_{\text{Kp}} \leq \log R'_{\text{Kp},\odot}$ is only $\sim 10\%$. This consequence exclude the possibility for the existence of a considerable fraction (e.g., $\sim 1/3$) of ‘‘Maunder-minimum stars’’ such that having activities significantly lower than the current solar-minimum level as once suggested by Baliunas and Jastrow (1990).

Yet, some stars (only a minor fraction of the sample) do exist showing activities still lower than that of the solar-minimum level. Having examined such 8 low-activity stars, we found that they tend to include planet-host stars and have low Li abundances, from which we suspect that their activities are actually low as a result of intrinsically slow rotation. It would be an important task to clarify the behavior of their activity variations by long-term monitoring observations.

⁴ As a comparatively well studied case where a sufficient amount of data are available, we may presumably state that HIP 96901 = HD 186427 showed a Sun-like cyclic variation in the 1995–2007 period; cf. figure 7 of Hall et al. (2007).

References

- Baliunas, S. L., et al. 1995, *ApJ*, 438, 269
Baliunas, S., & Jastrow, R. 1990, *Nature*, 348, 520
Cox, A. N. 2000, *Allen's Astrophysical Quantities*, 4th ed. (Berlin: Springer)
Duncan, D. K., et al. 1991, *ApJS*, 76, 383
Eddy, J. A. 1976, *Science*, 192, 1189
Hall, J. C., & Lockwood, G. W. 2004, *ApJ*, 614, 942
Hall, J. C., Lockwood, G. W., & Skiff, B. A. 2007, *AJ*, 133, 862
Isaacson, H., & Fischer, D. 2010, *ApJ*, 725, 875
Kurucz, R. L. 1993, Kurucz CD-ROM, No. 13 (Harvard-Smithsonian Center for Astrophysics) [also available at <http://kurucz.harvard.edu/PROGRAMS.html>]
Kurucz, R. L., & Bell, B. 1995, Kurucz CD-ROM, No. 23 (Harvard-Smithsonian Center for Astrophysics) [also available at <http://kurucz.harvard.edu/LINELISTS.html>]
Noguchi, K., et al. 2002, *PASJ*, 54, 855
Noyes, R. W., Hartmann, L. W., Baliunas, S. L., Duncan, D. K., & Vaughan, A. H. 1984, *ApJ*, 279, 763
Strassmeier, K., Washuettl, A., Granzer, Th., Scheck, M., & Weber, M. 2000, *A&AS*, 142, 275
Takeda, Y., Honda, S., Kawanomoto, S., Ando, H., & Sakurai, T. 2010, *A&A*, 515, A93 (Paper II)
Takeda, Y., Kawanomoto, S., Honda, S., Ando, H., & Sakurai, T. 2007, *A&A*, 468, 663 (Paper I)
Takeda, Y., Tajitsu, A., Honda, S., Kawanomoto, S., Ando, H., & Sakurai, T. 2011, *PASJ*, 63, 697 (Paper III)
Vaughan, A. H., & Preston, G. W. 1980, *PASP*, 92, 385
Vaughan, A. H., Preston, G. W., Wilson, O. C. 1978, *PASP*, 90, 267
Wright, J. T. 2004, *AJ*, 128, 1273
Wright, J. T., Marcy, G. W., Butler, R. P., & Vogt, S. S. 2004, *ApJS*, 152, 261

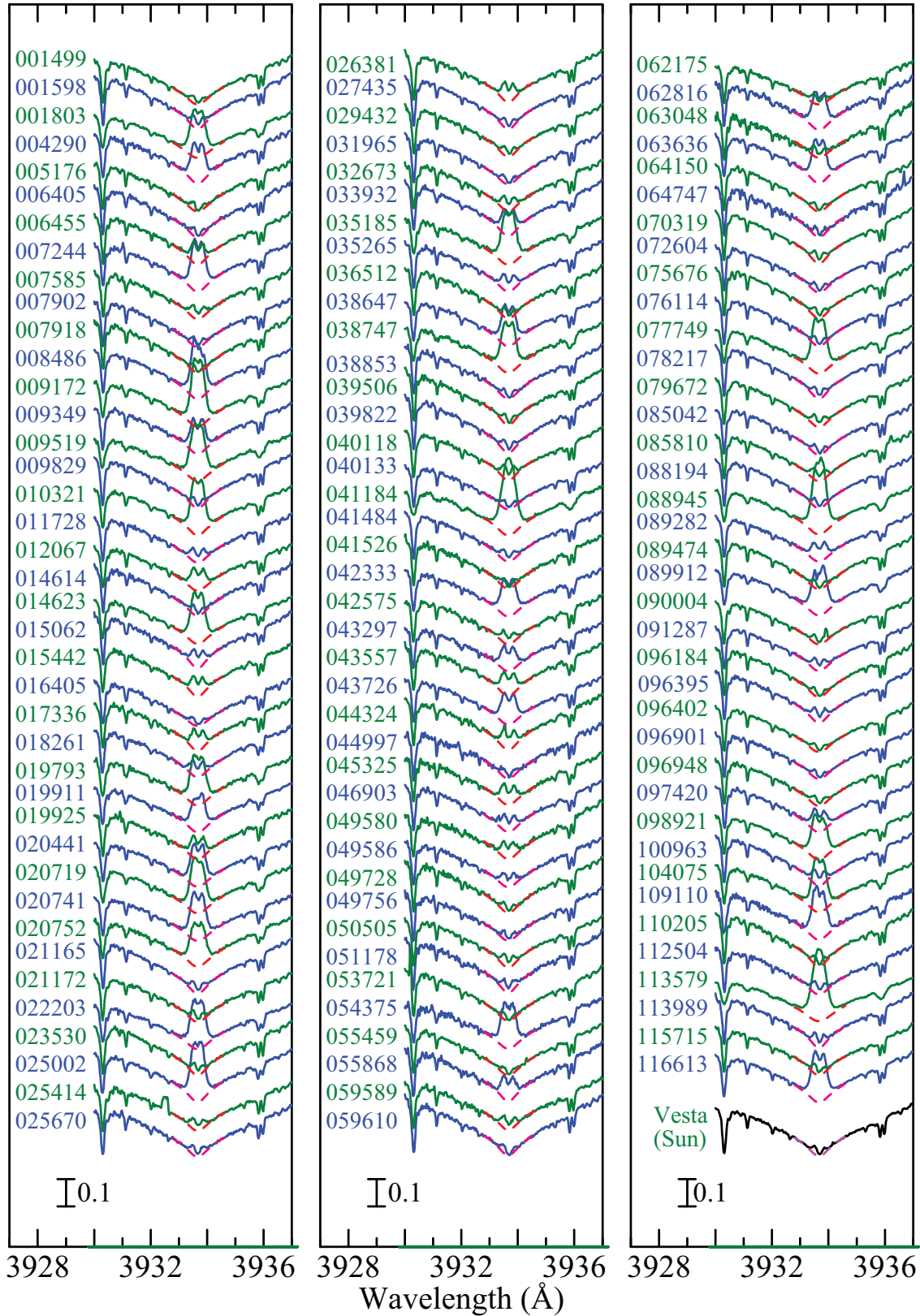


Fig. 2. Display of the 3930–3937 Å region spectra (r_{λ}^{obs}) of the Ca II K line at 3933.663 Å for all the 118 program stars along with the Vesta/Sun, where the theoretical line profile (r_{λ}^{th}) calculated from the solar photospheric model is also overplotted by (red) dashed line in the core region (3932.8–3934.6 Å) around the line center. Each spectrum is vertically shifted by 0.1 (in continuum unit) relative to the adjacent one. The wavelength scale of all stellar spectra is adjusted to the laboratory frame by correcting the radial velocity shifts. The HIP numbers are indicated in the figure.

Table 1. Activity index, rotation, Li abundance, age, and the atmospheric parameters.

HIP	$\log R'_{\text{Kp}}$	$r_0(8542)$	$v_e \sin i$	$A(\text{Li})$	$A(\text{Be})$	$\log \text{age}$	T_{eff}	$\log g$	v_t	[Fe/H]	Remark
001499	-5.32	0.190	2.01	(<1.1)	1.42	9.59	5724	4.45	0.95	+0.20	
001598	-5.12	0.222	1.94	1.81	1.10	9.98	5693	4.33	0.96	-0.27	
001803	-4.32	0.389	5.55	2.65	1.42	8.88	5817	4.41	1.17	+0.24	
004290	-4.50	0.320	2.34	2.18	1.14	9.44	5719	4.40	1.10	-0.12	
005176	-5.28	0.195	2.52	1.89	1.37	9.33	5855	4.39	1.03	+0.19	
006405	-5.33	0.213	2.07	1.71	1.24	9.55	5728	4.38	0.96	-0.14	
006455	-4.81	0.227	1.41	1.74	1.27	9.43	5716	4.57	0.99	-0.09	
007244	-4.39	0.351	2.31	2.29	1.23	9.56	5755	4.52	1.12	-0.04	
007585	-5.06	0.209	2.34	1.84	1.35	9.68	5784	4.50	1.04	+0.07	
007902	-5.31	0.182	2.13	(<0.9)	1.28	9.39	5613	4.39	0.91	-0.01	
007918	-5.42	0.191	2.57	1.89	1.25	9.56	5841	4.30	1.12	+0.01	
008486	-4.34	0.311	2.41	2.55	1.33	9.69	5805	4.45	1.13	-0.06	
009172	-4.25	0.282	4.29	2.50	1.37	9.47	5763	4.56	1.12	+0.06	
009349	-4.54	0.245	2.26	2.06	1.14	9.73	5788	4.35	1.07	+0.01	
009519	-4.27	0.465	6.94	2.97	1.50	9.29	5853	4.45	1.22	+0.14	
009829	-5.31	0.211	1.77	(<0.9)	1.03	10.03	5579	4.25	0.94	-0.31	
010321	-4.34	0.395	3.27	2.50	1.35	9.41	5707	4.60	1.04	-0.01	
011728	-5.04	0.205	2.11	(<1.0)	1.27	9.48	5708	4.40	1.02	+0.02	
012067	-4.71	0.240	1.97	(<1.3)	1.44	9.42	5709	4.41	0.96	+0.20	
014614	-5.21	0.220	2.49	1.58	1.20	9.58	5726	4.26	1.00	-0.12	
014623	-4.36	0.389	3.31	2.00	1.35	9.49	5742	4.52	1.09	+0.12	
015062	-4.96	0.222	2.32	2.02	1.10	9.47	5735	4.49	0.94	-0.29	
015442	-4.89	0.233	1.80	1.67	1.18	9.70	5682	4.50	0.87	-0.19	
016405	-5.32	0.184	2.65	(<1.2)	1.38	9.48	5738	4.32	1.03	+0.26	
017336	-4.87	0.164	2.07	(<0.8)	(<-0.9)	9.59	5671	4.55	0.94	-0.13	Be depleted
018261	-4.94	0.242	2.71	2.27	1.23	9.40	5873	4.43	0.97	+0.02	
019793	-4.32	0.385	5.17	2.53	1.35	9.23	5828	4.51	1.26	+0.19	
019911	-4.54	0.351	3.73	2.26	1.33	9.76	5672	4.34	1.10	-0.13	
019925	-4.75	0.262	2.39	1.61	1.34	9.47	5767	4.53	0.99	+0.07	
020441	-4.42	0.376	2.84	2.28	1.16	9.41	5771	4.42	1.10	+0.13	
020719	-4.30	0.462	5.40	2.60	1.29	9.27	5831	4.36	1.24	+0.13	
020741	-4.35	0.391	3.33	2.41	1.25	9.05	5797	4.37	1.20	+0.16	
020752	-4.38	0.375	4.63	2.72	1.40	9.28	5923	4.46	1.13	+0.16	
021165	-5.20	0.220	2.53	1.61	1.24	9.66	5760	4.28	0.99	-0.16	
021172	-5.23	0.196	1.85	(<1.0)	1.11	9.63	5625	4.27	0.90	-0.10	
022203	-4.36	0.340	3.92	2.30	1.27	9.55	5740	4.33	1.07	+0.13	
023530	-5.21	0.211	1.24	(<0.8)	0.84	9.94	5601	4.36	0.91	-0.24	
025002	-4.32	0.369	3.40	2.38	1.31	9.56	5729	4.47	1.07	-0.08	
025414	-5.13	0.220	1.85	(<1.1)	1.25	9.37	5635	4.49	0.89	+0.10	
025670	-5.19	0.218	2.05	(<1.2)	1.34	9.52	5759	4.55	0.88	+0.10	
026381	-4.98	0.240	0.96	(<0.7)	1.22	10.26	5518	4.47	0.87	-0.45	PHS, outlier in [Fe/H]/ T_{eff}
027435	-5.27	0.231	1.92	1.53	1.13	9.87	5697	4.45	0.93	-0.22	
029432	-5.27	0.200	2.14	1.06	1.12	9.67	5712	4.32	1.00	-0.12	
031965	-5.39	0.167	2.11	1.00	1.33	9.87	5770	4.31	0.99	+0.05	
032673	-5.02	0.176	1.83	(<1.0)	(<-0.8)	9.50	5724	4.57	0.95	+0.06	Be depleted
033932	-4.67	0.373	3.50	2.48	1.16	9.36	5891	4.38	1.10	-0.12	
035185	-4.33	0.444	4.81	2.71	1.29	9.76	5793	4.19	1.35	0.00	
035265	-4.92	0.191	1.77	2.01	1.15	9.79	5804	4.37	1.04	-0.02	
036512	-5.31	0.218	1.42	1.25	1.24	9.52	5718	4.49	0.89	-0.09	
038647	-4.47	0.315	2.55	2.13	1.30	9.43	5714	4.43	0.95	+0.01	
038747	-4.34	0.424	5.53	2.75	1.38	9.42	5804	4.42	1.05	+0.07	
038853	-5.31	0.222	2.53	2.44	1.16	9.60	5899	4.27	1.03	-0.05	
039506	-5.44	0.227	2.14	(<0.9)	1.06	10.36	5600	4.24	0.83	-0.62	outlier in [Fe/H]/ T_{eff}
039822	-5.19	0.231	1.97	(<1.2)	1.13	9.63	5758	4.35	0.90	-0.22	
040118	-5.12	0.202	1.36	(<0.9)	1.08	10.12	5541	4.45	0.84	-0.42	outlier in [Fe/H]/ T_{eff}
040133	-5.26	0.184	2.36	1.54	1.35	9.59	5698	4.33	0.97	+0.12	
041184	-4.18	0.545	10.32	2.83	1.70	9.45	5705	4.43	1.51	+0.11	
041484	-5.07	0.202	2.64	1.73	1.26	9.79	5864	4.33	0.92	+0.05	
041526	-5.24	0.222	2.13	2.03	1.23	9.78	5801	4.27	0.98	-0.02	
042333	-4.46	0.293	3.31	2.35	1.35	9.21	5816	4.44	1.08	+0.14	
042575	-5.07	0.236	2.03	1.17	1.28	9.42	5675	4.40	0.96	+0.06	
043297	-4.71	0.296	2.22	1.60	1.23	9.30	5691	4.46	1.05	+0.08	
043557	-4.73	0.255	3.28	1.50	1.19	9.80	5805	4.42	1.05	-0.06	
043726	-4.57	0.240	1.59	1.88	1.27	9.57	5769	4.48	1.01	+0.11	
044324	-4.80	0.285	2.35	2.41	1.27	9.34	5888	4.46	1.09	-0.01	
044997	-5.31	0.198	1.84	(<1.2)	1.32	9.49	5696	4.54	0.75	+0.04	
045325	-4.79	0.311	3.09	2.35	1.28	9.24	5935	4.47	0.97	+0.18	
046903	-4.89	0.238	2.91	2.02	1.22	9.53	5746	4.40	1.11	-0.03	
049580	-4.89	0.215	2.48	1.98	1.26	9.58	5782	4.41	0.87	+0.02	
049586	-4.98	0.222	2.21	(<1.3)	1.29	9.49	5786	4.42	1.06	+0.20	
049728	-5.34	0.175	2.01	(<1.0)	1.30	9.60	5744	4.40	0.98	-0.07	
049756	-5.29	0.185	2.14	1.34	1.21	9.58	5720	4.29	0.99	+0.02	
050505	-5.12	0.218	1.49	(<0.9)	1.25	9.85	5590	4.44	0.84	-0.17	
051178	-5.14	0.229	1.77	(<1.2)	0.80	9.66	5801	4.47	0.87	-0.17	
053721	-5.43	0.193	2.69	1.75	1.23	9.89	5819	4.19	1.15	-0.02	PHS
054375	-4.38	0.353	4.06	2.44	1.31	9.36	5803	4.37	0.96	+0.14	

Table 1. (Continued)

HIP	$\log R'_{\text{KP}}$	$r_0(8542)$	$v_e \sin i$	$A(\text{Li})$	$A(\text{Be})$	$\log age$	T_{eff}	$\log g$	v_t	[Fe/H]	Remark
055459	-5.34	0.218	2.39	1.58	1.37	9.58	5812	4.36	1.03	+0.07	
055868	-4.75	0.256	1.92	2.14	1.19	9.55	5757	4.49	0.95	-0.15	
059589	-5.13	0.205	1.81	(<1.2)	1.49	9.39	5654	4.52	0.70	-0.01	
059610	-5.40	0.229	2.22	1.62	1.23	9.63	5829	4.34	1.04	-0.06	PHS
062175	-5.12	0.198	2.52	1.83	1.34	9.53	5683	4.19	0.90	+0.13	
062816	-4.49	0.296	3.57	2.16	1.33	9.49	5804	4.44	0.97	+0.06	
063048	-5.26	0.189	1.81	(<1.1)	1.34	9.50	5655	4.32	0.91	-0.02	
063636	-4.45	0.351	2.93	2.26	1.23	9.62	5799	4.52	1.10	-0.01	
064150	-5.38	0.187	2.21	(<1.0)	(<-0.9)	9.63	5726	4.42	0.99	+0.05	Be depleted
064747	-5.40	0.204	1.77	(<1.1)	1.19	9.80	5710	4.42	0.93	-0.18	
070319	-5.23	0.207	1.56	1.09	1.20	10.07	5678	4.42	0.96	-0.33	
072604	-5.28	0.191	2.26	(<1.1)	1.31	10.03	5655	4.24	0.84	-0.14	
075676	-5.19	0.200	2.18	(<1.1)	(<-1.0)	9.62	5772	4.44	0.88	-0.08	Be depleted
076114	-5.29	0.195	1.76	0.91	1.22	9.59	5709	4.42	1.02	-0.02	
077749	-4.27	0.416	4.77	2.70	1.56	9.22	5836	4.61	1.14	+0.22	
078217	-5.22	0.213	1.17	1.89	1.15	9.54	5749	4.43	1.10	-0.22	
079672	-5.12	0.193	2.34	1.63	1.30	9.66	5768	4.40	0.96	+0.04	
085042	-5.33	0.187	2.01	(<0.8)	1.34	9.43	5676	4.48	0.99	+0.03	
085810	-5.05	0.193	2.86	2.05	1.35	9.43	5856	4.46	1.08	+0.15	
088194	-5.32	0.196	1.78	(<0.8)	1.25	9.67	5693	4.33	0.98	-0.08	
088945	-4.20	0.558	6.51	(<1.1)	-0.19	9.73	5800	4.38	1.44	-0.01	outlier in $A(\text{Li})$
089282	-4.80	0.240	3.41	2.45	1.22	9.34	5833	4.22	1.00	0.00	
089474	-5.30	0.189	2.50	(<0.9)	1.25	9.89	5755	4.20	1.04	+0.01	
089912	-4.36	0.436	6.04	2.69	1.42	9.43	5846	4.38	1.24	+0.04	
090004	-5.25	0.176	1.76	(<1.2)	1.33	9.83	5607	4.42	0.85	-0.02	PHS
091287	-5.07	0.185	2.05	1.74	1.34	9.21	5648	4.46	0.88	-0.01	
096184	-5.34	0.165	2.03	1.65	1.40	9.25	5863	4.45	1.00	+0.13	
096395	-5.02	0.218	2.30	2.18	1.25	9.76	5816	4.48	1.00	-0.10	
096402	-5.32	0.182	1.99	(<1.1)	1.28	9.90	5661	4.20	1.00	-0.03	
096901	-5.38	0.185	1.97	(<1.1)	1.37	9.77	5742	4.32	1.01	+0.08	PHS
096948	-5.21	0.175	1.85	1.52	1.30	9.62	5725	4.36	1.07	+0.07	
097420	-4.72	0.209	2.57	2.22	1.41	9.65	5780	4.42	1.04	+0.05	
098921	-4.38	0.329	3.66	2.47	1.39	9.13	5810	4.50	1.19	+0.17	
100963	-4.97	0.200	2.39	1.72	1.24	9.71	5779	4.46	0.98	0.00	
104075	-4.31	0.409	5.01	2.72	1.32	9.20	5881	4.37	1.08	+0.05	
109110	-4.35	0.409	4.78	2.49	1.41	9.28	5835	4.51	1.11	+0.07	
110205	-5.31	0.216	1.98	1.09	1.12	9.96	5708	4.28	1.08	-0.23	
112504	-5.06	0.209	1.99	2.01	1.37	9.63	5741	4.34	1.00	+0.01	
113579	-4.20	0.573	10.31	3.06	1.49	9.57	5759	4.21	1.44	+0.05	
113989	-5.17	0.222	1.94	(<0.8)	0.99	10.13	5506	4.38	0.74	-0.46	outlier in $[\text{Fe}/\text{H}]/T_{\text{eff}}$
115715	-5.25	0.215	2.34	1.72	1.22	10.08	5684	4.15	1.05	-0.19	
116613	-4.32	0.349	2.96	2.12	1.22	8.95	5869	4.49	1.11	+0.16	
Sun/Vesta	-5.33	0.193	2.29	0.92	1.22	9.66	5761	4.44	1.00	-0.01	

Note. Following the HIP number in column 1, $\log R'_{\text{KP}}$ (column 2) is the emission-strength index of the Ca II K line determined in this study, $r_0(8542)$ (column 3) is the residual flux at the line center of the Ca II 8542 line (cf. Paper II), $v_e \sin i$ (column 4) is the projected rotational velocity in km s^{-1} calibrated in Paper II, $A(\text{Li})$ (column 5) as well as $A(\text{Be})$ (column 6) are the lithium and beryllium abundances derived in Papers I and III (in the usual normalization of $A(\text{H}) = 12.00$), and $\log age$ (column 7) is the logarithm of the stellar age (in yr) derived from theoretical evolutionary tracks in Paper I. In columns 8–11 are presented the atmospheric parameters for each star, which are the “standard parameters” derived from Fe I and Fe II lines (cf. section 3.1.1 in Paper I): T_{eff} (effective temperature: in K) $\log g$ (surface gravity; in cm s^{-2}), v_t (microturbulence; in km s^{-1}), and $[\text{Fe}/\text{H}]$ (metallicity defined by $A(\text{Fe}) - 7.50$, where $A(\text{Fe})$ is the logarithmic Fe abundance), respectively. In column 12 (remark), “PHS” denotes planet-host stars.